Available online at www.sciencedirect.com
SCIENCE DIRECT
Icarus 174 (2005) 192–204
ICARUS
www.elsevier.com/locate/icarus

Dynamical implications of Jupiter's tropospheric ammonia abundance

Adam P. Showman [a,*], Imke de Pater [b]

[a] *Department of Planetary Sciences, Lunar and Planetary Laboratory, University of Arizona, Tucson, AZ 85721, USA*
[b] *Department of Astronomy, University of California at Berkeley, 601 Campbell Hall, Berkeley, CA, USA*

Received 14 April 2004; revised 5 October 2004

Abstract

Groundbased radio observations indicate that Jupiter's ammonia is globally depleted from 0.6 bars to at least 4–6 bars relative to the deep abundance of ∼ 3 times solar, a fact that has so far defied explanation. The observations also indicate that (i) the depletion is greater in belts than zones, and (ii) the greatest depletion occurs within Jupiter's local 5-μm hot spots, which have recently been detected at radio wavelengths. Here, we first show that both the global depletion and its belt-zone variation can be explained by a simple model for the interaction of moist convection with Jupiter's cloud-layer circulation. If the global depletion is dynamical in origin, then important endmember models for the belt-zone circulation can be ruled out. Next, we show that the radio observations of Jupiter's 5-μm hot spots imply that the equatorial wave inferred to cause hot spots induces vertical parcel oscillation of a factor of ∼ 2 in pressure near the 2-bar level, which places important constraints on hot-spot dynamics. Finally, using spatially resolved radio maps, we demonstrate that low-latitude features exceeding ∼ 4000 km diameter, such as the equatorial plumes and large vortices, are also depleted in ammonia from 0.6 bars to at least 2 bars relative to the deep abundance of 3 times solar. If any low-latitude features exist that contain 3-times-solar ammonia up to the 0.6-bar ammonia condensation level, they must have diameters less than ∼ 4000 km.

Keywords: Jupiter, atmosphere; Atmospheres, dynamics; Atmospheres, composition; Radio observations

1. Introduction

Despite the progress that has been made in the past two decades in understanding Jupiter's tropospheric circulation (Ingersoll et al., 2004), the basic nature of the dark, cyclonic belts and bright, anticyclonic zones remains elusive. A key problem is the difficulty of characterizing the conditions below the 0.5-bar cloud deck; at visible and infrared wavelengths, only 5-μm photons can reach space from as deep as 5 bars, and these primarily derive from unusual, nearly cloud-free "5-μm hot spots" that cover only a small fraction of Jupiter's area. Radio observations provide a complementary, and under-utilized, resource in constraining the dynamics, because they are minimally affected by clouds and hence can sample globally—not just in hot spots—to pressures of 5 bars or deeper. Because the primary radio-wavelength opacity source is ammonia gas, radio observations can be used to infer Jupiter's tropospheric ammonia abundance far below its 0.6-bar condensation level (de Pater, 1986; Atreya et al., 1999).

The Galileo Probe's detection of 3–4 times solar ammonia at pressures exceeding 8 bars (Folkner et al., 1998; Wong et al., 2004) provides a conundrum for interpretation of radio brightness measurements of Jupiter. Radio-wavelength maps produced using Very Large Array telescope data at 2, 3.5, and 6 cm show brightness temperatures far exceeding that of an atmosphere with constant 3–4-times-solar abundance up to the 0.6-bar condensation level. Instead, the data require that, relative to the deep abundance, ammonia is globally depleted from the 0.6-bar condensation level down to 4–6 bars and is subsolar at pressures $p < 2$ bars (Fig. 1), with belts more strongly depleted than zones (de Pater et al., 2001). The global depletion is puzzling, because the simplest models for convection in

* Corresponding author. Fax: +1-520-621-4933.
E-mail address: showman@lpl.arizona.edu (A.P. Showman).

0019-1035/$ – see front matter
doi:10.1016/j.icarus.2004.10.004

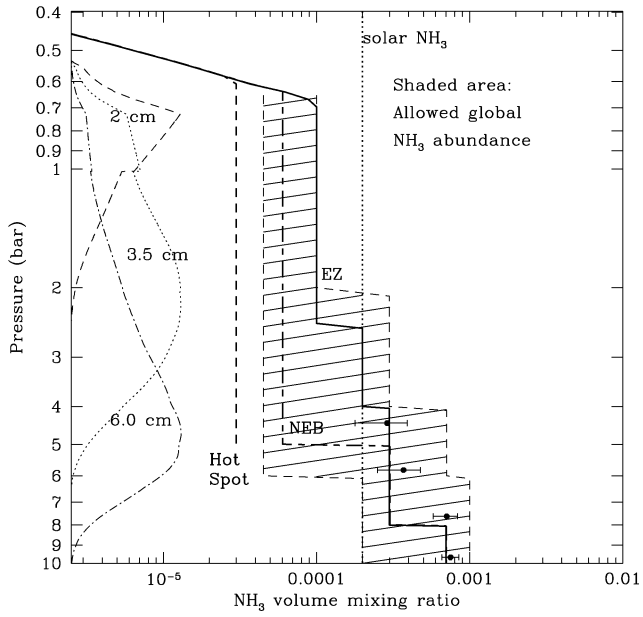

Fig. 1. The ammonia abundance on Jupiter consistent with radio observations at 2, 3.5, and 6 cm. The hatched area gives the allowed global abundance. The thick solid and dot-dashed lines show characteristic profiles in the Equatorial Zone (EZ) and North Equatorial Belt (NEB), respectively, that allow the brightness-temperature differences between the EZ and NEB at 2, 3.5, and 6 cm to be explained. The increase in ammonia abundance with depth and the ∼ 50–70% difference between the EZ and NEB are robust, although the exact location of the various steps in the two profiles are not (see de Pater et al., 2001). The thick dashed curve gives the mean abundance from 1–4 bars in 5-μm hot spots from Sault et al. (2004). Sault's retrieval provided only a mean mole fraction, represented in the plot as a vertical line, but more likely the abundance increases with depth as in the EZ and NEB. To schematically illustrate the expected decrease caused by condensation in the cloud layer, the curves follow the saturation profile above the condensation level. The vertical dotted line is the solar abundance and the filled circles are Galileo probe data from Folkner et al. (1998). The 2, 3.5, and 6-cm weighting functions are illustrated at the left with thin dashed, dotted, and dot-dashed curves, respectively. After de Pater et al. (2001).

Jupiter's interior suggest that condensable vapors should be well-mixed up to the condensation level. Although the probe measured depleted conditions at pressures less than 8 bars, the probe entered an anomalously dry 5-μm hot spot that is not representative of Jupiter as a whole, and the mechanisms that cause local hot-spot drying are probably not applicable to the global belt-zone circulation (Atreya et al., 1996; Owen et al., 1996; Orton et al., 1998; Young, 1998, 2003; Showman and Ingersoll, 1998; Showman and Dowling, 2000). A distinct mechanism is therefore needed. To explain the global depletion from 0.6–2 bars, de Pater (1986) invoked ammonia sequestration into the solid NH_4SH cloud, which forms from reaction of gaseous ammonia and H_2S at pressures less than 2 bars (Weidenshilling and Lewis, 1973; Atreya and Romani, 1985; Carlson et al., 1987). Because the solar sulfur-to-nitrogen (S/N) ratio is ∼ 0.14, this mechanism can only deplete most of the ammonia if the H_2S/NH_3 ratio is ∼ 6 times solar. However, the Galileo probe showed that the H_2S/NH_3 ratio is nearly solar (Niemann et al., 1998; Folkner et al., 1998), so only one-sixth of the ammonia can be removed using this mechanism. de Pater et al. (2001) suggested that perhaps each H_2S molecule removes multiple NH_3 molecules, either through adsorption of the ammonia onto the NH_4SH aerosols or its incorporation into the crystal lattice, but detailed calculations suggest that such depletion is minimal (Romani et al., 2000). Furthermore, because NH_4SH condensation occurs only above the 2-bar level, such loss, if any, cannot explain the global depletion down to 4–6 bars. Loss of ammonia into an aqueous water cloud is another possibility, but cloud-chemistry calculations suggest that only a few percent of the ammonia can be removed in this way (Carlson et al., 1987). An explanation for the global depletion, therefore, has yet to be found. We here propose a dynamical solution to this conundrum, and we show that, if the ammonia depletion is dynamical in origin, it can rule out some hypotheses for the sub-cloud belt-zone structure while supporting others. This is the first published mechanism capable of explaining a global ammonia depletion down to the 4–6-bar level.

A further development is that Sault et al. (2004) have obtained the first longitudinally resolved maps of Jupiter's brightness temperatures at radio wavelengths; all previous radio maps were longitudinally averaged because of the multi-hour integration times required to achieve adequate signal-to-noise. Sault et al. (2004) developed a data-analysis technique that allows the longitudinal structure to be retained despite the long integration times. The Sault et al. (2004) maps show substantial low-latitude structure, including radio-bright hot spots that coincide with the 5-μm hot spots. Because these data are not affected by clouds, they can provide a firm comparison of the ammonia abundance between hot spots and their surroundings. In Section 3, we use these new data to help constrain the dynamics of Jupiter's 5-μm hot spots and equatorial plumes.

2. Belt-zone circulation and the global ammonia depletion

2.1. Observed belt-zone structure

Voyager, Galileo, and Cassini measurements define the belt-zone circulation above the ammonia clouds. Hazes, which extend from ∼ 200 to 600 mbar or deeper (depending on location), overlie a higher-opacity, spatially variable cloud deck whose mean optical depth is generally greater in zones than belts (West et al., 1986; Carlson et al., 1994), helping to explain the visual brightness of zones relative to belts. Galileo visible and near-infrared imaging data suggest that this cloud lies at ∼ 0.7 bars (Banfield et al., 1998; Simon-Miller et al., 2001), whereas Galileo NIMS infrared spectra suggest instead a cloud pressure of ∼ 1.4 bars (Irwin et al., 2001; Irwin and Dyudina, 2002). At 0.7 bars, the ammonia abundance correlates with cloud opacity (Gierasch et al., 1986), confirming the radio inference that belts have greater ammonia depletion than zones. At pressures less than

0.5 bars, Voyager measured low temperatures over zones and high temperatures over belts, implying through thermal-wind balance that the zonal jets decay with height above the clouds (Pirraglia et al., 1981; Conrath et al., 1981). At and above the clouds, these measurements are all well explained by a zonally symmetric, thermally indirect Hadley-cell circulation pattern, with ascent in zones and descent in belts (Gierasch et al., 1986; West et al., 1992; Moreno and Sedano, 1997). In zones, the rising air advects ammonia upward, leading to cloudy and ammonia-rich conditions; the low temperatures result from adiabatic cooling of the ascending air. In belts, the descending air advects ammonia-poor air downward and causes adiabatic compression, producing drier, warmer, and more cloud-free conditions.

Galileo images of lightning provide information on the belt-zone structure below the clouds. Galileo showed that the lightning occurs within rapidly expanding, opaque clouds that grow to diameters up to 2000–5000 km in a few days (Little et al., 1999; Gierasch et al., 2000); dozens of such storms were also imaged by Cassini (Porco et al., 2003). As evidenced by their visibility in the 889 nm methane band, the storm tops stand up to 50 km above the surrounding cloud deck. These thunderstorms are probably driven by condensation of water, as ammonia and H_2S are too scarce to drive thunderstorm-strength updrafts or cause cloud electrification (Gierasch and Conrath, 1985; Gibbard et al., 1995; Yair et al., 1995). The lightning occurs at altitudes $\sim$ 80–120 km below the ammonia clouds, at pressures of 5–10 bars (Borucki and Williams, 1986; Little et al., 1999; Dyudina et al., 2002), consistent with the water-condensation pressure of $\sim$ 6 bars. Furthermore, portions of the thunderstorm cloud tops have pressures exceeding 4 bars, where the only condensate is water (Banfield et al., 1998; Gierasch et al., 2000). Intriguingly, Voyager, Galileo, and Cassini showed that thunderstorms primarily occur in belts (Cook et al., 1979; Magalhaes and Borucki, 1991; Little et al., 1999; Porco et al., 2003).

2.2. Scenarios for sub-cloud belt-zone structure

The occurrence of thunderstorms in belts implies the existence of a large reservoir of convective available potential energy, or CAPE (Emanuel, 1994, pp. 169–171), that can be released by moist-convective motions. The requirement is a "conditionally stable" temperature profile, where the mean lapse rate from $\sim$ 1–6 bars lies between the moist and dry adiabats (Salby, 1996, p. 176), which inhibits dry convection below the water-condensation level but allows violent, episodic convection driven by latent-heat release when plumes occasionally rise to the lifting condensation level. Finite CAPE occurs commonly on Earth and may result from a variety of processes (Emanuel, 1994). In Jupiter's belts, the simplest configuration consists of descending air whose virtual potential temperature slightly exceeds that of Jupiter's deep adiabat, with an interface below the water condensation altitude (Fig. 2). This jump in virtual potential temperature

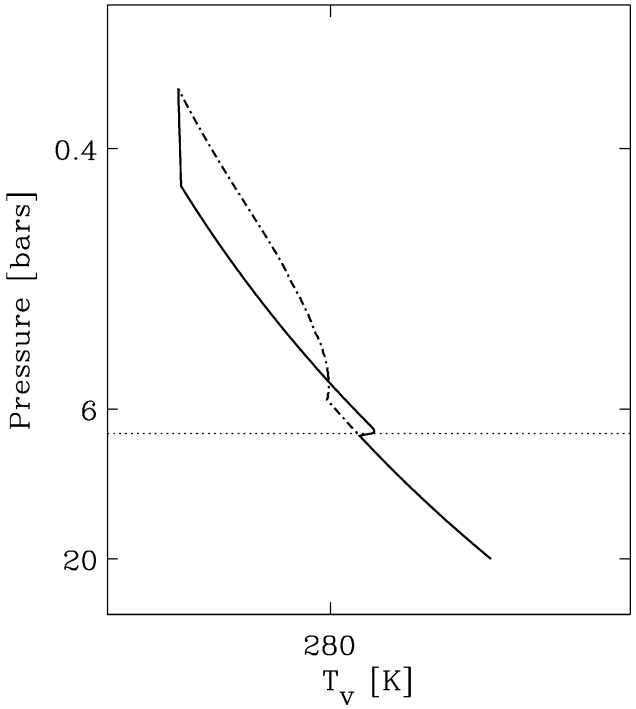

Fig. 2. Schematic temperature profile in Jupiter's belts (solid line) that allows finite CAPE, hence thunderstorms, to occur. Descending air cools radiatively at $p < 1$ bar, producing a statically stable region, but follows a dry adiabat below. Thunderstorms follow a moist adiabat (dash-dot line), which leads to large buoyancy. CAPE is the vertical integral of the difference between the dash-dot and solid lines. The interface between the descending air and the deep interior (dotted line) forms a stable layer that inhibits vertical mixing, so only rarely are plumes from the deep interior able to reach the water condensation level and trigger a thunderstorm. This allows CAPE to be maintained: the thunderstorms decrease CAPE, but in a statistical steady state they are rare enough for CAPE to be regenerated by the radiative cooling of the upper-tropospheric air. Although the interface between the subsiding air and the deep interior is shown as a sharp discontinuity (dotted line), it could also be vertically extended; the requirement for maintaining finite CAPE is simply that the air above the interface has greater virtual potential temperature than air below the interface and that the interface be deeper than the condensation level. The horizontal axis is virtual temperature, defined as $T_v = T m_d/m$, where T is temperature, m_d is the mass per molecule of dry air, and m is the mass per molecule of actual air including moisture. The difference between updrafts and downdrafts has been exaggerated for clarity.

forms a stable layer that inhibits convection across the interface, which is necessary to maintain CAPE. In contrast to the situation in belts, the lack of thunderstorms in Jupiter's zones implies either that the inhibiting stable layer is too deep, preventing any plumes from reaching the condensation level despite the existence of finite CAPE, or that CAPE is nearly zero in zones.

On Jupiter, two endpoint scenarios can reconcile the regions of thunderstorm activity with the upper tropospheric cloud and temperature pattern inferred from spacecraft data. In the first scenario, the zonally symmetric Hadley-cell circulation inferred to exist above the clouds extends to pressures of 6 bars or greater, driven by latent-heat release associated with the circulation (e.g., Barcilon and Gierasch,

1970). Large-scale upwelling occurs in zones and downwelling in belts, explaining the upper tropospheric ($p <$ 0.7 bar) belt-zone cloud and temperature patterns. As illustrated in Fig. 2, the subsidence in belts would produce a temperature structure that yields finite CAPE in belts, hence allowing thunderstorms there. Furthermore, we expect that the large-scale upwelling in zones would produce a moist-adiabatic profile there, implying that in this model CAPE in zones is nearly zero. Because convective plumes would not have the buoyancy needed to trigger violent updrafts, the lack of thunderstorms in zones is naturally explained by this scenario.

In a second scenario, Ingersoll et al. (2000) suggest that although net upwelling and downwelling occurs over zones and belts, respectively, at pressures less than 0.5 bars, the reverse occurs at the 6-bar water-condensation level. According to this picture, the ascending mass flux in belt thunderstorms dominates over the gradual subsidence between storms, leading to net ascent in belts at pressures of 1–6 bars. In belts, the vertical convergence of the net mass flow near ~ 1 bar requires a horizontal divergence, with a net belt-to-zone mass flow in the cloud layer. In zones, the resulting horizontal convergence causes vertical divergence that, in the extreme variant of the model, leads to descent at the 6-bar water condensation level. Ingersoll et al. (2000) proposed that the belt-to-zone mass flux is supplied by eddies—resulting from geostrophic adjustment of the thunderstorms—that are ejected from belts into zones by the so-called "beta gyre" effect (e.g., see LeBeau and Dowling, 1998; Li and Wang, 1994, for discussion of this effect). Jupiter's large vortices tend not to migrate in latitude (e.g., Rogers, 1995), but whether small-scale turbulence leads to a mean flow from belts to zones at cloud level has yet to be determined. In this scenario, the net ascent in belts from 1–6 bars cannot occur as a large-scale, belt-wide ascent, because that would produce thick zone-like stratus clouds and high water abundances, inconsistent with observations (e.g., Carlson et al., 1994; Bjoraker et al., 1986). Furthermore, it would lead to a moist-adiabatic environmental temperature profile and hence small CAPE, which would prevent thunderstorms from occurring in belts, inconsistent with lightning observations. Instead, the dry air subsiding from the upper troposphere in belts must penetrate to altitudes below the clouds, which would produce the relatively low cloud and water abundances observed in belts and lead to finite CAPE (Fig. 2), as necessary to explain the lightning. The net ascent in belts from 1–6 bars postulated in this scenario must therefore occur in thunderstorms and other local features. Although zones would have nonzero CAPE in this scenario, the net descent of air at 6 bars would push the stable layer too deep for thunderstorms to occur there.

2.3. Implications for tropospheric ammonia

Consider the implications of these scenarios for the tropospheric ammonia abundance. Both scenarios can explain an ammonia depletion down to 6 bars in belts: when the dry air descending from above the 0.5-bar level mixes with thunderstorm air containing the deep ammonia abundance of ~ 3 times solar, air containing 1–2 times solar ammonia (a ~ 2-fold depletion) is readily produced. If the thunderstorm anvils form at pressures less than 0.5 bars (as suggested by the observations; Gierasch et al., 2000), condensation and rainout of ammonia will occur within the thunderstorms, and subsidence of this ammonia-poor air can contribute to the depletion. Rapid mixing with the underlying reservoir of air containing the deep 3-times-solar ammonia abundance is prevented by the same stable layer that maintains the finite CAPE necessary for explaining the thunderstorms. Because this stable layer must be deeper than 6 bars, the ammonia depletion naturally extends to the 6-bar level, as required by the observations (de Pater et al., 2001). This picture is an extension of that proposed by Lunine and Hunten (1987) for the depletion of water.

The two scenarios have divergent predictions regarding the ammonia abundance within zones, however. In the first scenario, large-scale ascent within zones transports the deep abundance of ~ 3 times solar ammonia up to the cloud base. Formation of solid NH_4SH at 2 bars will decrease the abundance at higher altitudes by up to 20% (Carlson et al., 1987), although this may be offset by sublimation of ammonia particles settling from the overlying ammonia cloud. This endpoint scenario therefore cannot produce the observed ammonia depletion and so, assuming the ammonia depletion is dynamical in origin, this scenario is ruled out. In the second scenario, air transported laterally from belts into zones provides the sole source of moisture in zones from 1–6 bars. Because these eddies result from mixing of thunderstorm air with dry air in belts, the zones will have an ammonia abundance from 1–6 bars intermediate between that of the belts and the deep interior—that is, depleted relative to the deep ammonia abundance, but less so than in belts.

The two scenarios also make distinct predictions regarding the water cloud in zones. The large-scale upwelling at 6 bars in the first scenario would produce a widespread water stratus cloud within zones, whereas the large-scale descent in the second scenario would produce zones predominantly free of water clouds. Although radiative-transfer inferences on water clouds from infrared spectra are troubled by obscuration from the overlying clouds and instrumental effects, current analyses suggest that only isolated water clouds exist, with no widespread layer (e.g., Fouchet et al., 2000; Roos-Serote et al., 1999; Banfield et al., 1998), favoring the second scenario.

2.4. Semiquantitative model

A simple model illustrates the belt and zone ammonia abundances that can occur for specified mass fluxes between the belts, zones, and deep interior. We focus on the second scenario described above, because of the two endpoint scenarios, only the second can potentially explain the ob-

served ammonia depletion. Consider an isolated belt-zone pair within the layer between the 6-bar water-condensation level and a surface just above the 0.5-bar ammonia clouds. Let $\dot{M}_B^{\rm deep}$ and $\dot{M}_B^{\rm top}$ be the rates of mass transport (kg sec^{-1}) into the belt through the bottom and top boundaries; similarly, $\dot{M}_Z^{\rm deep}$ and $\dot{M}_Z^{\rm top}$ are the rates of mass transport out of the zone through the bottom and top boundaries. $\dot{M}^{\rm side}$ is the net horizontal transport from belt to zone (Fig. 3). All mass transports are defined positive. Mass conservation within the belt requires

$$\dot{M}_B^{\rm deep} + \dot{M}_B^{\rm top} - \dot{M}^{\rm side} = 0 \tag{1}$$

with a similar relation holding for zone transports. Mass conservation though the 6- and 0.5-bar surfaces require $\dot{M}_B^{\rm deep} = \dot{M}_Z^{\rm deep}$ and $\dot{M}_B^{\rm top} = \dot{M}_Z^{\rm top}$, respectively, so we henceforth drop subscripts on the mass transports. If we assume that air transported into belts from below contains the deep ammonia abundance and that the eddies transported laterally out of belts contain the mean belt ammonia abundance, then ammonia conservation in the belt requires

$$r f_{\rm deep} \dot{M}^{\rm deep} - f_B \dot{M}^{\rm side} = 0, \tag{2}$$

where f_B and $f_{\rm deep}$ are the ammonia mole fractions in the belt and the deep interior, respectively. The descending air above the 0.5-bar level is essentially ammonia free, so no ammonia is transported into belts from above. r is an empirical factor ($0 \leqslant r \leqslant 1$) to allow for rainout of ammonia in the belt thunderstorms; if 30% of the ammonia condenses and falls through the 6-bar surface, then $r \approx 0.7$. ($1 - r$ is essentially the precipitation efficiency.) Ammonia conservation in the zone requires

$$f_B \dot{M}^{\rm side} - f_Z \dot{M}^{\rm deep} = 0. \tag{3}$$

The large-scale ascent at 0.5 bars leads to ammonia condensation, and because the particle settling time is short compared to the $\sim 10^8$-sec overturn time for the circulation (Carlson et al., 1988), no ammonia is lost through the top boundary. These relationships imply

$$f_B = r f_{\rm deep} \left(1 + \frac{\dot{M}^{\rm top}}{\dot{M}^{\rm deep}}\right)^{-1} \tag{4}$$

and

$$f_Z = r f_{\rm deep}. \tag{5}$$

These relationships imply that, if no rainout of ammonia occurs in the thunderstorms, then zones are not depleted—although air entering zones from the sides has an ammonia abundance less than the deep abundance, the condensation that occurs at 0.5 bars acts as a concentrator that leads to a mean abundance equal to the deep abundance. Belts, however, are depleted by a factor of $1 + \dot{M}^{\rm top}/\dot{M}^{\rm deep}$ relative to the deep abundance. We can estimate $\dot{M}^{\rm top}/\dot{M}^{\rm deep}$ as follows. Dynamical and radiative-transfer analyses of Hubble Space Telescope and Voyager data imply that the mean vertical velocity at 270 mbar is $\sim 10^{-4}$ m sec^{-1}, upward in zones and downward in belts (Moreno and Sedano, 1997; West et al., 1992). With a density at 270 mbar of 0.06 kg m^{-3}, the vertical mass flux across that surface is $\sim 6 \times 10^{-6}$ kg m^{-2} sec^{-1}, upward in zones and downward in belts. The mass flux at 6 bars is less certain, but we can derive an estimate from the requirement that the motions transport Jupiter's internal heat flux. Let the updraft mass flux in belts (e.g., associated with thunderstorms and other local regions of ascent) averaged over the belt area be $\dot{m}$ and the mean temperature difference between updrafts and downdrafts be ΔT. The mean updraft mass flux is then $\dot{m} \sim F/c_p \Delta T$, where F is the heat flux. The existence of thunderstorms suggests that ΔT is large. If the background static stability is small, as in Fig. 2, then condensation of 3 times solar water implies $\Delta T \sim 10$ K. If the water abundance is 10 times solar, as has been suggested to explain the propagation speed of waves observed after the Shoemaker–Levy 9 impact (Ingersoll and Kanamori, 1995), then ΔT could be as large as 30 K. Adopting $F \sim 5$ W m^{-2} (relevant to Jupiter's low latitudes) and $c_p = 1.3 \times 10^4$ J kg^{-1}K^{-1}, we obtain net mass fluxes of 4×10^{-5} and 1.3×10^{-5} kg m^{-2} sec^{-1} for 3 and 10 times solar water, respectively. As a consistency check, we can calculate the bottom mass flux directly from the Voyager and Galileo observations of thunderstorm size and frequency, following Banfield et al. (1998) and Gierasch et al. (2000). For example, the Galileo data imply the average frequency of storms in belts is 7×10^{-10} km^{-2} (Little et al., 1999), and the measured divergence rate within a typical storm (i.e., the rate of growth of the storm cloud's area) was 20 km^2 sec^{-1} (Gierasch et al., 2000). If this divergence rate is typical, and if the expanding cloud extends across a range of pressures of ~ 0.5 bar, then the mean upward mass flux is 3×10^{-5} kg m^{-2} sec^{-1}, similar to the theoretical estimate. (In effect this agreement amounts to a statement that much of the internal heat can be carried by localized thunderstorms, as occurs on Earth; see Banfield et al., 1998; Gierasch et al., 2000.) These estimates suggest that $\dot{M}^{\rm top}/\dot{M}^{\rm deep} \sim 0.1$–$0.5$, implying that 10–50% ammonia depletion occurs in belts if no ammonia rainout occurs from the thunderstorms.

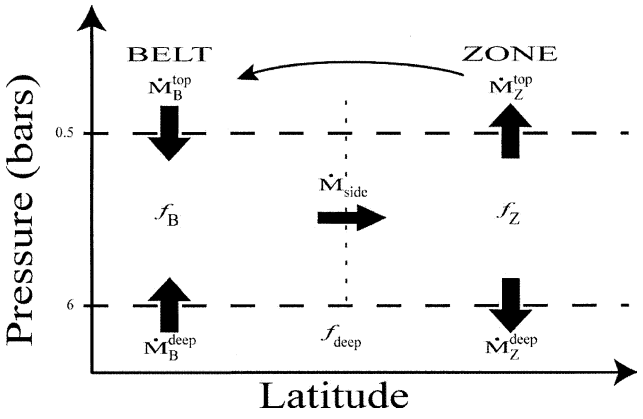

Fig. 3. Schematic illustration of the model (Eqs. (1)–(5)) used to estimate the belt and zone ammonia depletion. See the text.

If ammonia rainout occurs in the belt thunderstorms, then belts and zones are depleted by an additional factor r. A variety of observational and modeling studies have been conducted to determine the precipitation efficiency of thunderstorms and frontal systems on Earth. The precipitation efficiency (defined as the ratio of water vapor mass that enters a storm to the condensed water mass that exits the bottom of the storm averaged over the storm's lifetime) can range from $\sim$ 20–90%, with values of 40–60% being typical for thunderstorm complexes and squall lines (e.g., Hobbs et al., 1980; Gamache and Houze, 1983; Fankhauser, 1988; Cotton et al., 1989; Chong and Hauser, 1989; Ferrier et al., 1996). On Jupiter, condensates coagulate rapidly into large droplets (Rossow, 1978; Carlson et al., 1988; Yair et al., 1995), and the large diameter of jovian storms would help to inhibit detrainment of condensate out the sides of the storm, which would lead to larger precipitation efficiencies than typically occur on Earth. Lunine and Hunten (1987) proposed that the low tropospheric water abundance observed by Bjoraker et al. (1986) occurs because the precipitation efficiency for water in jovian storms is $\sim$ 99%. In contrast to water, the high volatility of ammonia implies that ammonia particles are unlikely to survive the descent to the 5-bar level unless the particle sizes exceed 1 cm (i.e., hail-sized). Such large particle sizes are probably unlikely. If, however, unidentified chemical mechanisms exist that can incorporate ammonia into the water or NH_4SH aerosols, then the rainout of the water through the 5-bar level would remove the ammonia as well. Alternatively, a substantial fraction of the storm's ammonia budget may be transported out the bottom of the storm as vapor in moist downdrafts. On Earth, moist downdrafts are a ubiquitous feature of thunderstorms; as rain falls into underlying air, it evaporates, and the evaporative cooling and precipitation mass loading increases the air density enough to initiate convective-scale moist downdrafts (Knupp and Cotton, 1985; Cotton and Anthes, 1989, Chapter 9). In long-lived, self-sustaining terrestrial thunderstorms, the updrafts and downdrafts become tilted so that the updraft overlies the downdraft. Precipitation formed in the updraft falls into the downdraft, which strengthens and maintains both drafts and allows them to coexist throughout the storm lifetime, which is often much longer than the time required for individual air parcels to traverse the storm. The extreme size and expansion rates, extensive lightning, and long lifespan of observed jovian storms suggest that these storms produce substantial precipitation, opening the possibility that the storms generate long-lived downdrafts too. If ammonia evaporation into such downdrafts leads to a downdraft ammonia mole fraction exceeding the deep mole fraction, then these storm will remove their own ammonia from the 0.6–6-bar layer even if no ammonia particles reach the 6-bar level before evaporating. To quantify this idea, we reworked Eqs. (1)–(5) to include the mass and ammonia fluxes of thunderstorm moist downdrafts. The new equations for conservation of mass, belt ammonia, and zone ammonia, respectively, read

$$\dot{M}_B^{\text{deep}} + \dot{M}_B^{\text{top}} - \dot{M}^{\text{side}} - \dot{M}^{\text{down}} = 0, \tag{6}$$

$$r f_{\text{deep}} \dot{M}_B^{\text{deep}} - f_B \dot{M}^{\text{side}} - f_{\text{down}} \dot{M}^{\text{down}} = 0, \tag{7}$$

$$f_B \dot{M}^{\text{side}} - f_Z (\dot{M}_B^{\text{deep}} - \dot{M}^{\text{down}}) = 0, \tag{8}$$

where $\dot{M}^{\text{down}}$ is the downward mass transport (kg sec^{-1}) across the 5-bar surface in thunderstorm moist downdrafts and f_{down} is the ammonia mole fraction in these downdrafts. This term appears only in the equation for the belt ammonia budget because thunderstorms are observed predominantly in belts (e.g., Porco et al., 2003; Little et al., 1999). If we further define a parameter $\delta \equiv \dot{M}^{\text{down}} / \dot{M}_B^{\text{deep}}$, then the solutions can be written

$$f_Z = \frac{r f_{\text{deep}} - \delta f_{\text{down}}}{1 - \delta} \tag{9}$$

and

$$f_B = \frac{r f_{\text{deep}} - \delta f_{\text{down}}}{1 - \delta + \dot{M}^{\text{top}} / \dot{M}_B^{\text{deep}}}. \tag{10}$$

These equations imply that, even if all ammonia particles evaporate ($r = 1$), factor-of-two ammonia depletion in zones can still occur as long as the downdraft ammonia mole fraction exceeds a critical value of $0.5 f_{\text{deep}}(1 + \delta^{-1})$. If the downdraft mass transport rate is 30–50% of the updraft mass transport rate, which is plausible, then factor-of-two ammonia depletion in zones will occur if downdrafts contain 1.5–2 times the deep ammonia mole fraction. Such ammonia abundances can plausibly be supplied to jovian-storm downdrafts as long as (1) the storm reaches sufficient altitudes for most of the ammonia to condense and (2) $\sim$ 50% of the ammonia particles rain down into the storm interior and enter moist downdrafts rather than being detrained out the storm sides. If gaseous ammonia primarily condenses into ammonia ice, then the first condition requires the thunderstorm anvils to form at pressures less than $\sim$ 0.5 bars (which seems to be the case for many jovian thunderstorms; Gierasch et al., 2000). However, if solid NH_4SH formation removes most of the gaseous ammonia, then anvil formation at pressures less than 2 bars is sufficient. The second condition results from the fact that the *maximum* downdraft ammonia abundance, f_{deep}/δ (corresponding to complete transfer of storm updraft ammonia into downdrafts), is approximately twice that needed to obtain factor-of-two ammonia depletion; factor-of-two depletion of ammonia can therefore occur if downdrafts remove only half of the ammonia. An open issue is whether evaporation of falling ammonia ice can initiate moist downdrafts, or whether evaporation of water is required, and if the latter, whether the downdrafts initiate at a high-enough altitude for sufficient ammonia ice to enter the downdrafts. Existing jovian thunderstorm models are not yet sophisticated enough to answer these questions. Yair et al.'s (1992, 1995) models are axisymmetric, which precludes the inherently three-dimensional structure of tilted

updrafts and downdrafts needed for strong supercell-type storms. Hueso and Sánchez-Lavega's (2001, 2004) simulations, while three-dimensional, do not account for precipitation settling and evaporation, which again precludes moist-downdraft formation. More work is needed to resolve these issues.

As with Eqs. (1)–(5), Eqs. (9)–(10) imply that belts have lower ammonia abundance than zones. For $\delta = 0.5$, $f_{\rm down} = 1.5 f_{\rm deep}$, $\dot{M}^{\rm top}/\dot{M}_B^{\rm deep} = 0.2$, and $r = 1$ (no rainout), for example, the equations imply that belts and zones have 36 and 50% of the deep ammonia mole fraction, respectively. The fractional depletion in belts relative to zones when downdrafts are included *exceeds* that when they are not included: the ratio of belt-to-zone ammonia mole fraction is now less than $(1 + \dot{M}^{\rm top}/\dot{M}_B^{\rm deep})^{-1}$. This effect can help contribute to the observed belt-zone ammonia contrast. In the model without downdrafts (Eqs. (4)–(5)), the ratio of $\dot{M}^{\rm top}/\dot{M}_B^{\rm deep}$ needed to attain a belt-to-zone ammonia ratio f_B/f_Z is $(f_Z/f_B) - 1$, so if we want $f_B/f_Z = 0.66$ (i.e., belts have two-thirds the ammonia abundance of zones), then we must have $\dot{M}^{\rm top}/\dot{M}_B^{\rm deep} = 0.5$. This ratio of $\dot{M}^{\rm top}/\dot{M}_B^{\rm deep}$, while possible, is at the upper limit of plausible values. When downdrafts are included, however, the required mass-transport ratio is decreased to $\dot{M}^{\rm top}/\dot{M}_B^{\rm deep} = [(f_Z/f_B) - 1](1 - \delta)$. If $\delta = 0.5$, then attaining $f_B/f_Z = 0.66$ requires only $\dot{M}^{\rm top}/\dot{M}_B^{\rm deep} = 0.25$. Therefore, including downdrafts allows belt-zone ammonia contrasts to be produced more easily for a given value of $\dot{M}^{\rm top}/\dot{M}_B^{\rm deep}$. Notice also that the belt-to-zone ammonia ratio depends only on the downdraft mass-transport rate and *not* on the ammonia mole fraction in the downdrafts.

The box model we have adopted, while informative, is simple, and one could wonder whether alternate assumptions about the ammonia exchange between belts, zones, and the deep interior would produce the same results. In Eqs. (2), (3), (7), and (8), we parameterized the ammonia transport using the reasonable idea that mass transported from one region to another carries with it the ammonia mole fraction from the source region. An alternate view might postulate that mass transported from one region to another takes with it an ammonia mole fraction equal to the mean ammonia mole fractions of the two regions (e.g., the ammonia transported from the deep interior to belts would then be $\dot{M}_B^{\rm deep}(f_B + f_{\rm deep})/2$ rather than $\dot{M}_B^{\rm deep} f_{\rm deep}$). In our opinion, this scheme lacks consistency with the physics of advection, which is the mechanism that causes the ammonia transport. Advection implies that air carries with it the trace-constituent concentrations of the source region; air moving from one region A to another region B cannot take with it the mole fraction from region B, or even the average of the mole fractions from regions A and B, because there is no way for the advected air to have foreknowledge of the destination before it arrives there. Nevertheless, in Eqs. (2), (3), (7), and (8), we allowed ammonia transport only from the deep interior to belts to zones to the deep interior, and neglected the reverse transport from the deep interior to zones to belts (Fig. 3). In reality, such reverse flows could occur in addition to the primary flows we assumed, and in that case it would not be possible to write the *net* ammonia transport from A to B as the *net* mass transport times the ammonia mole fraction of A (where here A and B each represent either belt, zone, or deep interior). To address this shortcoming, we derive in Appendix A the belt and zone ammonia mole fractions allowing for the possibility of these additional mass fluxes, whose magnitudes we represent as free parameters. Over a wide range of parameter values, we find that, as with our simpler model, f_B is less than f_Z, and both are depleted relative to the deep abundance if thunderstorm moist downdrafts exist. This result gives us confidence that, at least within the box-model context, our results are robust.

In summary, loss of thunderstorm ammonia through the 6-bar level—from direct rainout, incorporation of ammonia into water and NH_4SH particles that rain out, or evaporation of ammonia into supermoist downdrafts that reach > 6 bars—would lead to a global depletion of ammonia in the 0.6–6-bar layer, with enhanced depletion in belts relative to zones. If 50% loss of thunderstorm ammonia occurs through the above mechanisms, which is plausible, then the ammonia would be depleted by a mean factor of ~ 2 in zones, and 2.2–3 in belts, from 1–6 bars. Therefore, under plausible conditions, a global ammonia depletion from 1–6 bars that is consistent with the radio observations, with a greater depletion in belts than zones, can be generated by atmospheric dynamics.

The observations suggest that the ammonia mole fraction increases with depth from 1–6 bars (Fig. 1). The abundances are probably supersolar at pressures exceeding ~ 4 bars, but values as low as half-solar in the equatorial zone and ~ 0.2–0.3 times solar in the north-equatorial belt are inferred from 0.6–2 bars. Relative to the deep abundance of 3-times solar, these numbers imply 2–3-fold ammonia depletion from $\sim$ 3–6 bars and 5–10-fold depletion from 0.6–2 bars. Our box model can only explain five-fold or greater ammonia depletions if $> 90\%$ of the ammonia rains out of thunderstorms, which we view as unlikely. However, the ammonia mole fractions in our model are essentially mass-weighted vertical averages from 0.6–6 bars. The observed mass-weighted ammonia depletion from 0.6–6 bars is two-to-three-fold and, as discussed earlier, our model can explain such depletion under plausible conditions. Nevertheless, the observed downward-increasing ammonia abundance needs explaining. In belts, such a downward-increasing abundance would naturally result from the fact that the background environmental air gradually subsides; deeper air would have spent longer in the 0.6–6-bar layer than shallower air, giving it more time to gain ammonia through detrainment from thunderstorms. Belt eddies transported laterally into zones would preserve this structure, giving zones a downward-increasing gradient too. It is also possible that evaporation of falling ammonia rain or detrainment of ammonia from small cumulus clouds in the 3–6-bar region causes higher ammo-

nia abundance from 3–6 bars than exists in the 0.5–2-bar layer.

3. Equatorial hot spots and plumes

The Galileo probe entered a 5-μm hot spot, one of approximately 10 regularly spaced cloud-free regions at 7° N latitude, and measured extremely dry conditions extending ∼ 80 km below the condensation levels (Young, 1998, 2003; Orton et al., 1998). Ammonia and H_2S reached constant values at 8 and 16 bars, respectively, while water was only 30% solar—and still increasing—at 20 bars (Niemann et al., 1998; Wong et al., 2004). Recent work (Showman and Dowling, 2000; Friedson and Orton, 1999; Ortiz et al., 1998) suggests that the hot spots result from a large-amplitude equatorially trapped wave that propagates westward relative to the flow. Air columns that enter the hot spot from the side undergo vertical stretching that pushes initially high-altitude air downward, causing clouds to sublimate and explaining the dry conditions measured by the probe. This column stretching provides the best explanation for the layered profiles of ammonia, H_2S, and water observed along the probe trajectory (Showman and Ingersoll, 1998), but the amount of column stretching that has occurred—hence the amplitude of the wave—remains unknown. If the initial (unstretched) air columns follow a simple condensation profile, with the deep condensable-gas abundances nearly constant up to the condensation levels and following saturation profiles at lower pressures, then explaining the extent of dryness measured by the probe requires that the air columns stretched downward by a factor of 5–10 in pressure (Showman and Ingersoll, 1998). The required stretching would be less, however, if the initial unstretched column were depleted relative to the condensation model. This issue is critical for understanding hot spot dynamics, because hot-spot behavior depends strongly on the wave amplitude (Showman and Dowling, 2000).

Here we use the spatially resolved radio maps (Sault et al., 2004) to constrain the stretching amplitude. Sault et al. (2004) showed that the 2-cm brightness temperature of the hot spots exceeds that of the surroundings by 20 K, and from these data they estimated that, from 1–4 bars, the hot-spot ammonia abundance is half that of the surroundings at the same pressure. The hot spots produce this decrease over time by downward advection of dry air. Let f be the ammonia mole fraction. If the rate of increase of f with pressure $\partial \ln f / \partial \ln p$ in the environment is approximately constant, then the difference in ammonia between pressure p_0 and a greater pressure p_1 can be expressed as

$$\Delta \ln f \sim \frac{\partial \ln f}{\partial \ln p} \Delta \ln p, \tag{11}$$

where $\Delta \ln f \equiv \ln f_1 - \ln f_0$, $\Delta \ln p \equiv \ln p_1 - \ln p_0$, and f_0 and f_1 are the ammonia abundances at pressures p_0 and p_1, respectively. In the hot spots, a drying is produced by downward advection of dry, high-altitude air. If the hot spot advects air from p_0 to p_1 while conserving ammonia, then the difference in ammonia between the environment and the hot spot at pressure p_1 is just $\Delta \ln f$ as given above.

Figure 1 shows the globally averaged ammonia abundances vs pressure from the radio observations (de Pater et al., 2001). The allowed abundance can be fit with a power-law increase of ammonia with pressure:

$$f = f_0 \left(\frac{p}{p_0} \right)^{\alpha} \tag{12}$$

with $\alpha \equiv \partial \ln f / \partial \ln p$. From Eq. (11), this yields a value of $\Delta \ln p \sim \Delta \ln f / \alpha$. The radio data imply that, globally, the transition to the deep 3-times-solar abundance must occur at a pressure exceeding 4 bars, but globally the transition is probably not reached deeper than 8 bars, since that would imply global conditions drier than the hot spot, inconsistent with a variety of measurements. Under the assumption that the ammonia abundance outside hot spots connects to the Galileo measurement of 3.5 times solar between 4–10 bars, and that α is constant from 1–10 bars, then $\alpha \sim 1.3$; values substantially higher or lower force the profile outside the allowable range of ammonia abundance. Sault et al.'s (2004) estimate that hot spots have half the ammonia abundance at the same pressure implies that $\Delta \ln f = 0.7$. This yields $\Delta \ln p \sim 0.5$ and implies that the pressure increases by a factor of ~ 1.6 during the subsidence. Because the 2-cm radio maps have a weighting function that extends from 1–4 bars, the stretching applies to these pressures. It is possible that the equatorial-zone ammonia abundance increases more slowly with depth from 1–4 bars, perhaps with α as low as 0.5, and then undergoes a rapid increase to three times solar at $p > 5$ bars; if so, the factor-of-two lower ammonia abundance in hot spots would yield $\Delta \ln p$ up to 1.4, implying a four-fold increase in pressure as air columns enter hot spots. Unless water is globally depleted below its condensation level, however, four-fold or greater stretching amplitudes are still required at pressures exceeding 6 bars in order to explain the water depletion measured by the probe (Showman and Ingersoll, 1998). Interestingly, Showman and Dowling (2000) showed that two-fold stretching produces behavior similar to actual hot spots; the effect of four-fold or greater stretching on hot-spot behavior has yet to be investigated. The hot-spot ammonia depletion from Sault et al. (2004) was derived for a large hot spot $7000 \times 14{,}000$ km in size, which appears to be fully resolved by the radio maps (see Fig. 4 of Sault et al., 2004), so the inferred stretching amplitude best applies to large hot spots. Small hot spots are not fully resolved in the radio maps, so we cannot determine whether they would have similar stretching amplitudes.

We next consider the implications of the radio maps for equatorial plumes. The plumes are wedge-shaped clouds, 10^4 km long, that lie between and somewhat equatorward of the hot spots. Early models for the plumes viewed them as gigantic thunderstorm anvils (Stoker, 1986) and emphasized the active plume heads that appeared to represent moist convection (Hunt et al., 1981, 1982). These plume heads, which

are typically 1000–2000 km across—much smaller than the plumes themselves—occurred on only a few plumes during the Voyager era and have been even less active during other epochs. More recent models (Allison, 1990) suggest that the plumes result from a planet-encircling, equatorially trapped wave, which is probably the same wave that induces hot spots (Showman and Dowling, 2000). The downward phase of the wave causes hot spots, while the upward phase of the wave leads to condensation and forms the equatorial plumes. The wave and convection ideas are not mutually exclusive; for example, the wave-induced ascent could occasionally trigger buoyant convection that leads to active plume heads from time to time. Nevertheless, the recent picture differs sharply from Stoker's (1986) view of plumes as thunderstorm anvils. Stoker's view implies that air in the plume cloud funneled upward from the deep atmosphere through plume-head thunderstorms before expanding laterally into the plume. In contrast, Allison's (1990) and Showman and Dowling's (2000) models imply that the air underneath the entire plume undergoes large-scale wave-induced ascent, and that the plumes constitute huge stratus clouds produced by this forced lifting. Plume heads may occur but are not necessary. These models would be aided by information about the atmospheric structure within plumes, but because of the large plume-cloud optical depth (Stoker and Hord, 1985), little is known about the structure of the plumes below the clouds. In particular, it is unknown whether ammonia is depleted in the air underlying the plume cloud.

The radio maps can provide important constraints on the ammonia abundance in the plumes and other local regions of uplift. de Pater et al. (2001) clearly showed that the *global mean* abundance is depleted from ~ 0.5–5 bars, but it has been unclear whether *local* regions containing 3-times solar ammonia can still exist. At 2 cm wavelength, Jupiter's disk-averaged brightness temperature is 165 K (Gibson et al., 2005), and because limb darkening affects the disk average temperature, the brightness temperature at the center of the disk may reach ~ 170 K. In contrast, we calculate that a region containing 3-times-solar ammonia up to 0.7 bars would produce a 2-cm brightness temperature of 152 K at the center of the disk, which is much colder than any region within the radio maps in Sault et al. (2004). The map resolution is about 1–2 arcsec, corresponding to a resolution of 2000–4000 km near the center of Jupiter's disk. Thunderstorms or other features less than ~ 1000 km in diameter are not resolved by the maps, and if these features contained 3-times-solar ammonia up to the ammonia cloud, small (< 10 K) brightness temperature signatures, which are consistent with the data, would result. However, any low-latitude features with diameters exceeding 4000 km are fully resolved. If they contained 3-times-solar ammonia up to the ammonia cloud, a 15–20 K depression in the 2-cm brightness temperature would result, and this is not observed. The equatorial plumes have dimensions of ~ 5000 by 10,000 km, large enough to be resolved in the radio maps. The implication is that the equatorial plumes cannot have 3-times-solar ammonia up to the 0.7-bar ammonia cloud base. However, this analysis does not rule out the possibility that the 1000–2000 km-diameter active plume *heads* observed during the Voyager era (Hunt et al., 1981, 1982) have 3-times solar ammonia up to the ammonia condensation level.

Intriguingly, Cassini CIRS analyses indicate that at 400 mbar the equatorial zone relative humidity is nearly 100% (Achterberg et al., manuscript in preparation). In contrast, the depletion discussed here refers to pressures exceeding the 0.7-bar cloud base. The two estimates are consistent if, in zones, ascent occurs at pressures < 0.7 bar and descent occurs at pressures > 1 bar, as proposed by Ingersoll et al. (2000). See Section 2 for discussion.

4. Conclusions

A simple model for the interaction of moist convection with Jupiter's large-scale circulation appears capable of explaining Jupiter's global, vertically averaged ammonia depletion at pressures of 0.6–5 bars as seen in groundbased radio data. To succeed, the model requires (1) that the majority of air that ascends across the 5-bar surface resides in isolated thunderstorms, and (2) that $\sim 50\%$ of the am-

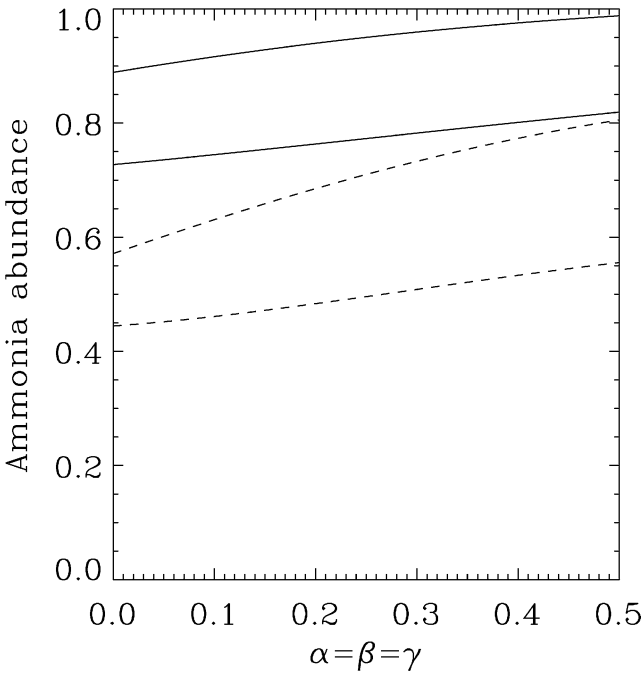

Fig. 4. Ammonia mole fractions from 1–5 bars in the belts and zones for the box-model solutions of Eqs. (A.5)–(A.8). Abscissa is relative strength of the deep-interior → zone → belt circulation that opposes the assumed primary deep-interior → belt → zone circulation (represented by α, β, and γ, where are assumed equal here; see the text). Ordinate gives ratio of ammonia mole fraction to the deep mole fraction. The solid curves assume $\delta = 0.1$ and the dashed curves assume $\delta = 0.3$. In each case, the upper curve gives $f_Z/f_{\rm deep}$ and the lower curve gives $f_B/f_{\rm deep}$. All the curves assume $\dot{M}^{\rm top}/\dot{M}_B^{\rm deep} = 0.2$, $f_{\rm down} = 2f_{\rm deep}$, and $r = 1$ (no rainout).

monia within these storms is lost through the 4–6-bar level by either direct ammonia rainout through the base of the storms or downward transport of ammonia vapor in convective downdrafts moistened by evaporation of rainfall. These conditions are plausible, although additional studies are necessary to determine whether they are actually satisfied. If the ammonia depletion indeed results from atmospheric dynamics, then these conditions rule out large-scale, gradual ascent through the 5-bar level in either belts or zones, because such motions would transport the deep, 3-times-solar ammonia abundance into the 1–5-bar region. The air undergoing large-scale ascent above the 0.5-bar cloud tops in zones is therefore probably supplied horizontally from belts (where thunderstorms predominantly occur) rather than from below, consistent with the scenario of Ingersoll et al. (2000). The zone-belt Hadley circulation above the 0.5-bar cloud tops can modulate the ammonia depletion, producing an additional depletion in belts of 10–50% depending on the mass flux of the circulation. This can help to explain the observation that belts are more depleted than zones by $\sim 50\%$. It is possible that an unidentified chemical mechanism exists that could deplete the ammonia, and if so, the dynamical mechanisms discussed here could interact with the chemical sink to strengthen and spatially modulate the depletion. For example, if the majority of ammonia is lost into the NH_4SH or H_2O clouds, then dynamics could force the depletion to greater depths than would otherwise occur and induce a belt-zone difference in ammonia that would otherwise not exist.

The longitudinally resolved 2-cm radio maps of Sault et al. (2004) place constraints on the ammonia abundance, hence dynamics, of equatorial hot spots, plumes, and large, low-latitude vortices. The two-fold ammonia depletion in hot spots relative to the surroundings suggests that the equatorial Rossby wave inferred to cause hot spots induces parcel oscillations of a factor of 1.5 to 4 in pressure, with a value of ~ 2 being most likely. Equatorial plumes and large vortices are, like Jupiter itself, depleted in ammonia near the 2-bar level; no low-latitude features larger than 4000-km diameter have the deep, 3-times-solar ammonia abundance all the way to the 0.5-bar ammonia clouds.

Acknowledgments

We thank Peter Gierasch for a helpful review and Virginia Smith for preparing Fig. 3. This work was supported by the NSF Planetary Astronomy program through grant number AST-0206269 and the NASA Planetary Atmospheres program through grant number NAG5-12062.

Appendix A

Here we consider a generalized box model for an isolated belt-zone pair that allows not only the mass transports considered in Fig. 3 but, in addition, belt-to-deep-interior, zone-to-belt, and deep-interior-to-zone mass transports. Let the magnitudes of these transports be $\alpha\dot{M}_B^{\rm deep}$, $\beta\dot{M}^{\rm side}$, and $\gamma\dot{M}_Z^{\rm deep}$, respectively, where $\dot{M}_B^{\rm deep}$, $\dot{M}^{\rm side}$, and $\dot{M}_Z^{\rm deep}$ are the deep-interior-to-belt, belt-to-zone, and zone-to-deep-interior transports. All transports are defined positive. We also include thunderstorm moist downdrafts, which transport mass from belts to the deep interior. Except for the thunderstorm downdrafts, each mass transport carries with it the ammonia mole fraction of the source region (f_B, f_Z, or $f_{\rm deep}$). We continue to allow the possibility of rainout in belt thunderstorms, but we do not allow rainout or moist downdrafts in the deep-interior-to-zone transport under the assumption that the deep-interior-to-zone transports are not thunderstorms. The belt-mass, zone-mass, belt-ammonia, and zone-ammonia conservation equations are then

$$(1-\alpha-\delta)\dot{M}_B^{\rm deep} - (1-\beta)\dot{M}^{\rm side} + \dot{M}^{\rm top} = 0, \tag{A.1}$$

$$-(1-\gamma)\dot{M}_Z^{\rm deep} + (1-\beta)\dot{M}^{\rm side} - \dot{M}^{\rm top} = 0, \tag{A.2}$$

$$(rf_{\rm deep} - \alpha f_B - \delta f_{\rm down})\dot{M}_B^{\rm deep} - (f_B - \beta f_Z)\dot{M}^{\rm side} = 0, \tag{A.3}$$

$$(\gamma f_{\rm deep} - f_Z)\dot{M}_Z^{\rm deep} + (f_B - \beta f_Z)\dot{M}^{\rm side} = 0. \tag{A.4}$$

This equation set implies that

$$f_Z = \frac{f_{\rm deep}(\gamma\alpha + \gamma\xi + r\chi\xi) - f_{\rm down}\chi\xi\delta}{\alpha + \xi(1+\alpha\chi\beta)} \tag{A.5}$$

and

$$f_B = \frac{rf_{\rm deep} - \delta f_{\rm down} + \beta\xi f_Z}{\alpha + \xi}, \tag{A.6}$$

where f_Z in Eq. (A.6) is given by Eq. (A.5). For simplicity we have defined

$$\chi \equiv \frac{1-\gamma}{1-\alpha-\delta} \tag{A.7}$$

and

$$\xi \equiv \frac{1-\alpha-\delta}{1-\beta} + \frac{1}{1-\beta}\frac{\dot{M}^{\rm top}}{\dot{M}_B^{\rm deep}}. \tag{A.8}$$

These solutions are valid as long as $\alpha + \xi \neq 0$, $\alpha + \delta \neq 1$, and $\alpha + \xi(1+\alpha\chi\beta) \neq 0$. For $\alpha = \beta = \gamma = \delta = 0$, the model collapses to that described in Fig. 3 and Eqs. (A.5)–(A.6) simplify to Eqs. (4)–(5). Similarly, if $\alpha = \beta = \gamma = 0$ but δ is nonzero, the equations become identical to Eqs. (9)–(10).

Figure 4 shows the zone and belt ammonia mole fractions for the simplified case of $\alpha = \beta = \gamma$. The figure demonstrates that f_Z exceeds f_B over a wide parameter range, consistent with the radio observations that belts have less ammonia than zones. The total ammonia depletion declines as the deep-interior → zone → belt circulation becomes stronger (counteracting the primary deep-interior → belt → zone circulation that is assumed), but substantial ammonia depletion still occurs in both belts and zones (allowed by the inclusion of thunderstorm moist downdrafts).

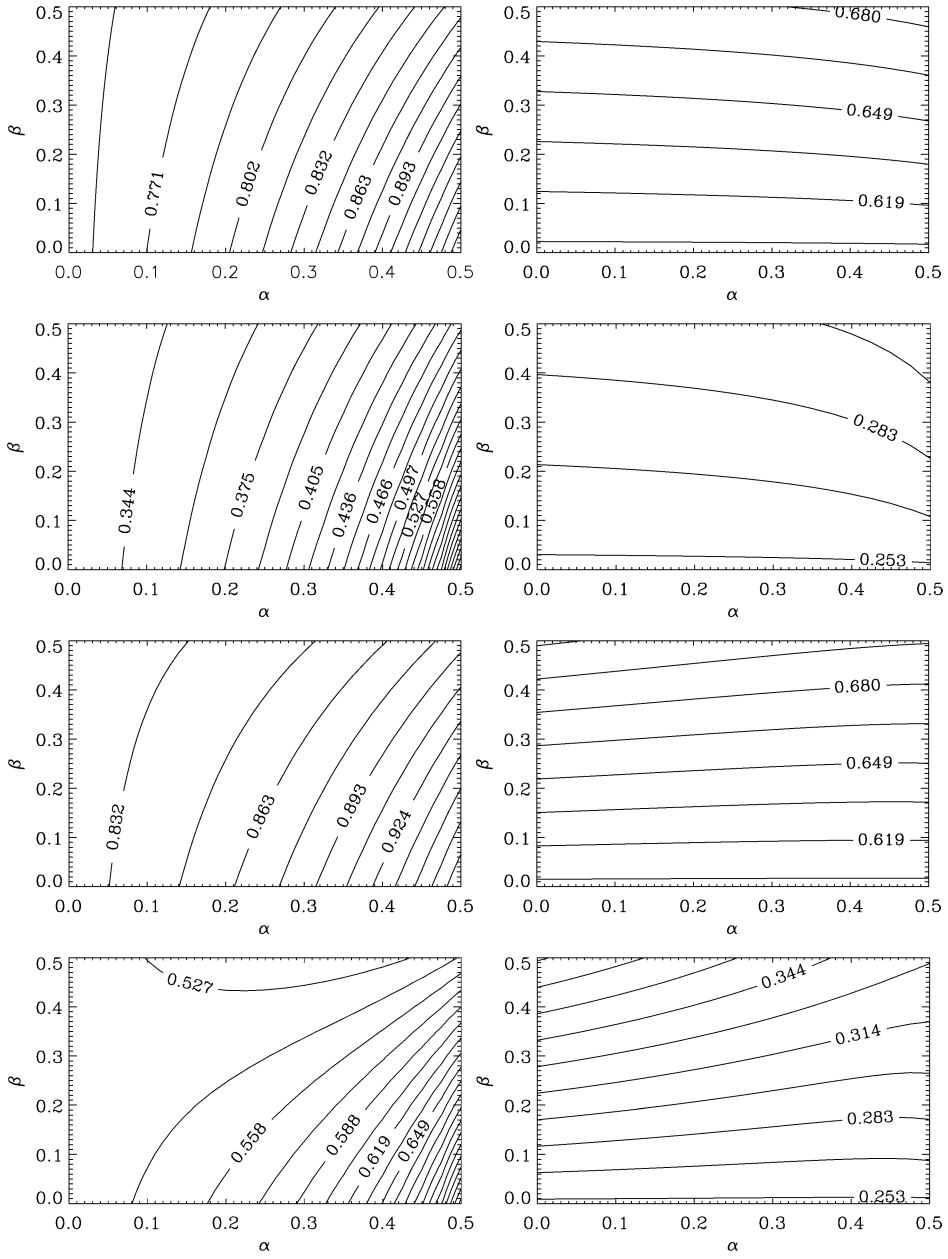

Fig. 5. Ammonia mole fractions versus α and β for different assumptions about γ and δ. The panels in the left column show contours of $f_Z/f_{\rm deep}$ and those in the right column shows $f_B/f_{\rm deep}$. Within each panel, γ and δ are held constant. In each column, from top to bottom, the panels assume (γ, δ) values of (0, 0.2), (0, 0.4), (0.3, 0.2), and (0.3, 0.4), respectively. All panels assume $\dot{M}^{\rm top}/\dot{M}_B^{\rm deep} = 0.2$, $f_{\rm down} = 2f_{\rm deep}$, and $r = 1$ (no rainout). The contour interval is 0.01525 throughout all panels. Comparison of the left and right panels within a given row shows that, for given values of α, β, γ, and δ, both zones and belts are depleted relative to the deep abundance, and that the depletion is stronger in belts than zones.

Figure 5 shows contour plots of the zone and belt ammonia abundances (left and right columns, respectively) for the more general case where α, β, and γ are unequal. Each panel depicts contours as a function of α and β for a given γ and δ; different panels adopt different values of γ and δ. Inspection of the figure shows that, as before, f_Z exceeds f_B and that both are depleted relative to the deep abundance. These figures show that the qualitative results obtained using the simpler models (Eqs. (1)–(5) and (6)–(10)) are robust to the inclusion of the additional mass and ammonia transports. As in Fig. 4, the depletion in zones results from the inclusion of moist downdrafts, and belts are additionally depleted because of the dry air that subsides from above.

References

Allison, M., 1990. Planetary waves in Jupiter's equatorial atmosphere. Icarus 83, 282–307.

Atreya, S., Wong, M.H., Owen, T., Niemann, H., Mahaffy, P., 1996. Chemistry and clouds of the atmosphere of Jupiter: a Galileo perspective. In: Rahe, J., Barbieri, C., Johnson, T., Sohus, A. (Eds.), Three Galileos: The

Man, the Spacecraft, the Telescope (conference proceedings). Kluwer Academic, Dordrecht.

Atreya, S.K., Wong, M.H., Owen, T.C., Mahaffy, P.R., Niemann, H.B., de Pater, I., Drossart, P., Encrenaz, Th., 1999. A comparison of the atmospheres of Jupiter and Saturn: deep atmospheric composition, cloud structure, vertical mixing, and origin. Planet. Space Sci. 47, 1243–1262.

Atreya, S.K., Romani, P.N., 1985. Photochemistry and clouds of Jupiter, Saturn, and Uranus. In: Hunt, G.E. (Ed.), Planetary Meteorology. Cambridge Univ. Press, Cambridge, pp. 17–68.

Barcilon, A., Gierasch, P., 1970. A moist, Hadley-cell model for Jupiter's cloud bands. J. Atmos. Sci. 27, 550–560.

Banfield, D., Gierasch, P.J., Bell, M., Ustinov, E., Ingersoll, A.P., Vasavada, A.R., West, R.A., Belton, M.J., 1998. Jupiter's cloud structure from Galileo imaging data. Icarus 135, 230–250.

Bjoraker, G.L., Larson, H.P., Kunde, V.G., 1986. The abundance and distribution of water vapor in Jupiter's atmosphere. Astrophys. J. 311, 1058–1072.

Borucki, W.J., Williams, M.A., 1986. Lightning in the jovian water cloud. J. Geophys. Res. Atmos. 91, 9893–9903.

Carlson, B.E., Prather, M.J., Rossow, W.B., 1987. Cloud chemistry on Jupiter. Astrophys. J. 322, 559–572.

Carlson, B.E., Rossow, W.B., Orton, G.S., 1988. Cloud microphysics of the giant planets. J. Atmos. Sci. 45, 2066–2081.

Carlson, B.E., Lacis, A.A., Rossow, W.B., 1994. Belt-zone variations in the jovian cloud structure. J. Geophys. Res. 99, 14623–14658.

Chong, M., Hauser, D., 1989. A tropical squall line observed during the COPT 81 experiment in West Africa. Part II. Water budget. Mon. Weather Rev. 117, 728–744.

Conrath, B.J., Flasar, F.M., Pirraglia, J.A., Gierasch, P.J., Hunt, G.E., 1981. Thermal structure and dynamics of the jovian atmosphere: 2. Visible cloud features. J. Geophys. Res. 86, 8769–8775.

Cook, A.F., Duxbury, T.C., Hunt, G.E., 1979. First results on jovian lightning. Nature 280, 794.

Cotton, W.R., Anthes, R.A., 1989. Storm and cloud dynamics. International Geophysics Series, vol. 44. Academic Press, San Diego.

Cotton, W.R., Lin, M.-S., McAnelly, R.L., Tremback, C.J., 1989. A composite model of mesoscale convective complexes. Mon. Weather Rev. 117, 765–783.

de Pater, I., 1986. Jupiter's zone-belt structure at radio wavelengths: II. Comparison of observations with model atmosphere calculations. Icarus 68, 344–365.

de Pater, I., Dunn, D., Romani, P., Zahnle, K., 2001. Reconciling Galileo probe data and ground-based radio observations of ammonia on Jupiter. Icarus 149, 66–78.

Dyudina, U.A., Ingersoll, A.P., Vasavada, A.R., Ewald, S.P., the Galileo SSI Team, 2002. Monte Carlo radiative transfer modeling of lightning observed in Galileo images of Jupiter. Icarus 160, 336–349.

Emanuel, K.A., 1994. Atmospheric Convection. Oxford Univ. Press, New York.

Fankhauser, J.C., 1988. Estimates of thunderstorm precipitation efficiency from Field measurements in CCOPE. Mon. Weather Rev. 116, 663–684.

Ferrier, B.S., Simpson, J., Tao, W.-K., 1996. Factors responsible for precipitation efficiencies in midlatitude and tropical squall simulations. Mon. Weather Rev. 124, 2100–2125.

Folkner, W.M., Woo, R., Nandi, S., 1998. Ammonia abundance in Jupiter's atmosphere derived from the attenuation of the Galileo probe's radio signal. J. Geophys. Res. Planets 103, 22847–22856.

Fouchet, T., Lellouch, E., Bézard, B., Encrenaz, T., Drossart, P., Feuchtgruber, H., de Graauw, T., 2000. ISO-SWS observations of Jupiter: measurement of the ammonia tropospheric profile and of the $^{15}N/^{14}N$ isotopic ratio. Icarus 143, 223–243.

Friedson, A.J., Orton, G.S., 1999. A dynamical model of Jupiter's 5-micron hot spot. Bull. Am. Astron. Soc. 31, 1155.

Gamache, J.F., Houze, R.A., 1983. Water budget of a mesoscale convective system in the Tropics. J. Atmos. Sci. 40, 1835–1850.

Gibbard, S., Levy, E.H., Lunine, J.I., 1995. Generation of lightning in Jupiter's water cloud. Nature 378, 592–595.

Gibson, J., Welch, W.J., de Pater, I., 2005. Accurate jovian radio flux density measurements show ammonia to be subsaturated in the upper troposphere. Icarus 173, 439–446.

Gierasch, P.J., Conrath, B.J., 1985. Energy conversion processes in the outer planets. In: Hunt, G. (Ed.), Recent Advances in Planetary Meteorology. Cambridge Univ. Press, Cambridge, pp. 120–146.

Gierasch, P.J., Conrath, B.J., Magalhaes, J.A., 1986. Zonal mean properties of Jupiter's upper troposphere from Voyager infrared observations. Icarus 67, 456–483.

Gierasch, P.J., Ingersoll, A.P., Banfield, D., Ewald, S.P., Helfenstein, P., Simon-Miller, A., Vasavada, A., Breneman, H.H., Senske, D.A., the Galileo imaging team, 2000. Observations of moist convection in Jupiter's atmosphere. Nature 403, 628–630.

Hobbs, P.V., Matejka, T.J., Herzegh, P.H., Locatelli, J.D., Houze, R.A., 1980. The mesoscale and microscale structure and organization of clouds and precipitation in midlatitude cyclones. I. A case study of a cold front. J. Atmos. Sci. 37, 568–596.

Hueso, R., Sánchez-Lavega, A., 2001. A three-dimensional model of moist convection for the giant planets: the Jupiter case. Icarus 151, 257–274.

Hueso, R., Sánchez-Lavega, A., 2004. A three-dimensional model of moist convection for the giant planets. II. Saturn's water and ammonia moist convective storms. Icarus 172, 255–271.

Hunt, G.E., Conrath, B.J., Pirraglia, J.A., 1981. Visible and infrared observations of jovian plumes during the Voyager encounter. J. Geophys. Res. 86, 8777–8781.

Hunt, G.E., Muller, J.-P., Gee, P., 1982. Convective growth rates of equatorial features in the jovian atmosphere. Nature 295, 491–494.

Ingersoll, A.P., Kanamori, H., 1995. Waves from the collisions of Comet Shoemaker–Levy 9 with Jupiter. Nature 374, 706–708.

Ingersoll, A.P., Gierasch, P.J., Banfield, D., Vasavada, A.R., the Galileo imaging team, 2000. Moist convection as an energy source for the large-scale motions in Jupiter's atmosphere. Nature 403, 630–632.

Ingersoll, A.P., Dowling, T.E., Gierasch, P.J., Orton, G.S., Read, P.L., Sánchez-Lavega, A., Showman, A.P., Simon-Miller, A.A., Vasavada, A.R., 2004. Dynamics of Jupiter's atmosphere. In: Bagenal, F., Dowling, T.E., McKinnon, W.B. (Eds.), Jupiter: Planet, Satellites, and Magnetosphere. Cambridge Univ. Press, Cambridge, pp. 105–128.

Irwin, P.G.J., Weir, A.L., Taylor, F.W., Calcutt, S.B., Carlson, R.W., 2001. The origin of belt/zone contrasts in the atmosphere of Jupiter and their correlation with 5-μm opacity. Icarus 149, 397–415.

Irwin, P.G.J., Dyudina, U., 2002. The retrieval of cloud structure maps in the equatorial region of Jupiter using a principal component analysis of Galileo/NIMS data. Icarus 156, 52–63.

Knupp, K.R., Cotton, W.R., 1985. Convective cloud downdraft structure: an interpretive survey. Rev. Geophys. 23, 183–215.

LeBeau, R.-P., Dowling, T.E., 1998. EPIC simulations of time-dependent, three-dimensional vortices with application to Neptune's Great Dark Spot. Icarus 132, 239–265.

Li, X., Wang, B., 1994. Barotropic dynamics of the beta gyres and beta drift. J. Atmos. Sci. 51, 746–756.

Little, B., Anger, C.D., Ingersoll, A.P., Vasavada, A.R., Senske, D.A., Breneman, H.H., Borucki, W.J., the Galileo SSI Team, 1999. Galileo images of lightning on Jupiter. Icarus 142, 306–323.

Lunine, J.I., Hunten, D.M., 1987. Moist convection and the abundance of water in the troposphere of Jupiter. Icarus 69, 566–570.

Magalhaes, J.A., Borucki, W.J., 1991. Spatial distribution of visible lightning on Jupiter. Nature 349, 311–313.

Moreno, F., Sedano, J., 1997. Radiative balance and dynamics in the stratosphere of Jupiter: results from a latitude-dependent aerosol heating model. Icarus 130, 36–48.

Niemann, H.B., Atreya, S.K., Carignan, G.R., Donahue, T.M., Haberman, J., Harpold, D., Hartle, R.E., Hunten, D.M., Kasprzak, W., Mahaffy, P., Owen, T.C., Way, S., 1998. The composition of the jovian atmosphere as determined by the Galileo probe mass spectrometer. J. Geophys. Res. 103, 22831–22846.

Ortiz, J.L., Orton, G.S., Friedson, A.J., Stewart, S.T., Fisher, B.M., Spencer, J.R., 1998. Evolution persistence of 5-μm hot spots at the Galileo probe entry latitude. J. Geophys. Res. 103, 23051–23069.

Orton, G.S., Fisher, B.M., Baines, K.H., Stewart, S.T., Friedson, A.J., Ortiz, J.L., Marinova, M., Ressler, M., Dayal, A., Hoffmann, W., Hora, J., Hinkley, S., Krishnan, V., Masanovic, M., Tesic, J., Tziolas, A., Parija, K.C., 1998. Characteristics of the Galileo probe entry site from Earth-based remote sensing observations. J. Geophys. Res. 103, 22791–22814.

Owen, T.C., 11 colleagues, 1996. Eos Spring Suppl. 77, S171.

Pirraglia, J.A., Conrath, B.J., Allison, M.D., Gierasch, P.J., 1981. Thermal structure and dynamics of Saturn and Jupiter. Nature 292, 677–679.

Porco, C.C., 23 colleagues, 2003. Cassini imaging of Jupiter's atmosphere, satellites, and rings. Science 299, 1541–1547.

Romani, P.N., de Pater, I., Dunn, D., Zahnle, K., Washington, B., 2000. Adsorption of ammonia onto ammonium hydrosulfide cloud particles in Jupiter's atmosphere. Bull. Am. Astron. Soc. 32, 997.

Roos-Serote, M., Drossart, P., Encrenaz, Th., Carlson, R.W., Leader, F., 1999. Constraints on the tropospheric cloud structure of Jupiter from spectroscopy in the 5-μm region: a comparison between Voyager/IRIS Galileo/NIMS and ISO/SWS spectra. Icarus 137, 315–340.

Rossow, W.B., 1978. Cloud microphysics: analysis of the clouds of Earth, Venus, Mars and Jupiter. Icarus 36, 1–50.

Salby, M.L., 1996. Fundamentals of Atmospheric Physics. Academic Press, San Diego.

Sault, R.J., Engel, C., de Pater, I., 2004. Longitude-resolved imaging of Jupiter at $\lambda = 2$ cm. Icarus 168, 336–343.

Showman, A.P., Ingersoll, A.P., 1998. Interpretation of Galileo probe data and implications for Jupiter's dry downdrafts. Icarus 132, 205–220.

Showman, A.P., Dowling, T.E., 2000. Nonlinear simulations of Jupiter's 5-micron hot spots. Science 289, 1737–1740.

Simon-Miller, A.A., Banfield, D., Gierasch, P.J., 2001. Color and the vertical structure in Jupiter's belts, zones, and weather systems. Icarus 154, 459–474.

Stoker, C.R., Hord, C.W., 1985. Vertical cloud structure of Jupiter's equatorial plumes. Icarus 64, 557–575.

Stoker, C.R., 1986. Moist convection: a mechanism for producing the vertical structure of the jovian equatorial plumes. Icarus 67, 106–125.

Weidenshilling, S.J., Lewis, J.S., 1973. Atmospheric and cloud structures of the jovian planets. Icarus 20, 465–476.

West, R.A., Strobel, D.F., Tomasko, M.G., 1986. Clouds, aerosols, and photochemistry in the jovian atmosphere. Icarus 65, 161–217.

West, R.A., Friedson, A.J., Appleby, J.F., 1992. Jovian large-scale stratospheric circulation. Icarus 100, 245–259.

Wong, M.H., Mahaffy, P.R., Atreya, S.K., Niemann, H.B., Owen, T.C., 2004. Updated Galileo probe mass spectrometer measurements of carbon, oxygen, nitrogen, and sulfur on Jupiter. Icarus 171, 153–170.

Yair, Y., Levin, Z., Tzivion, S., 1992. Water-cumulus in Jupiter's atmosphere: numerical experiments with an axisymmetric cloud model. Icarus 98, 72–81.

Yair, Y., Levin, Z., Tzivion, S., 1995. Lightning generation in a jovian thundercloud: results from an axisymmetric numerical cloud model. Icarus 115, 421–434.

Young, R.E., 1998. The Galileo probe mission to Jupiter: science overview. J. Geophys. Res. 103, 22775–22790.

Young, R.E., 2003. The Galileo probe: how it has changed our understanding of Jupiter. New Astron. Rev. 47, 1–51.